Title

Direct tests of cytochrome c and c1 functions in the electron transport chain of malaria parasites

Journal

Proceedings of the National Academy of Sciences of the United States of America, 120(19)

ISSN

0027-8424

Authors

Espino-Sanchez, Tanya J
Wienkers, Henry
Marvin, Rebecca G
et al.

Publication Date

2023-05-09

DOI

10.1073/pnas.2301047120

Peer reviewed

PNAS RESEARCH ARTICLE | MICROBIOLOGY
BIOPHYSICS AND COMPUTATIONAL BIOLOGY

Direct tests of cytochrome *c* and c_1 functions in the electron transport chain of malaria parasites

Tanya J. Espino-Sanchez[a,1], Henry Wienkers[a,1], Rebecca G. Marvin[a,1], Shai-anne Nalder[a], Aldo E. García-Guerrero[a], Peter E. VanNatta[b], Yasaman Jami-Alahmadi[c], Amanda Mixon Blackwell[a], Frank G. Whitby[a], James A. Wohlschlegel[c], Matthew T. Kieber-Emmons[b], Christopher P. Hill[a], and Paul A. Sigala[a,2]

Edited by L. David Sibley, Washington University in St Louis, St. Louis, MO; received January 24, 2023; accepted March 30, 2023

The mitochondrial electron transport chain (ETC) of *Plasmodium* malaria parasites is a major antimalarial drug target, but critical cytochrome (cyt) functions remain unstudied and enigmatic. Parasites express two distinct cyt *c* homologs (*c* and *c*-2) with unusually sparse sequence identity and uncertain fitness contributions. *P. falciparum* cyt *c*-2 is the most divergent eukaryotic cyt *c* homolog currently known and has sequence features predicted to be incompatible with canonical ETC function. We tagged both cyt *c* homologs and the related cyt c_1 for inducible knockdown. Translational repression of cyt *c* and cyt c_1 was lethal to parasites, which died from ETC dysfunction and impaired ubiquinone recycling. In contrast, cyt *c*-2 knockdown or knockout had little impact on blood-stage growth, indicating that parasites rely fully on the more conserved cyt *c* for ETC function. Biochemical and structural studies revealed that both cyt *c* and *c*-2 are hemylated by holocytochrome *c* synthase, but UV-vis absorbance and EPR spectra strongly suggest that cyt *c*-2 has an unusually open active site in which heme is stably coordinated by only a single axial amino acid ligand and can bind exogenous small molecules. These studies provide a direct dissection of cytochrome functions in the ETC of malaria parasites and identify a highly divergent *Plasmodium* cytochrome *c* with molecular adaptations that defy a conserved role in eukaryotic evolution.

mitochondria | malaria | *Plasmodium* | electron transport chain | cytochrome

Significance

Mitochondria are critical organelles in eukaryotic cells that drive oxidative metabolism. The mitochondrion of *Plasmodium* malaria parasites is a major drug target that has many differences from human cells and remains poorly studied. One key difference from humans is that malaria parasites express two cytochrome *c* proteins that differ significantly from each other and play untested and uncertain roles in the mitochondrial electron transport chain (ETC). Our study revealed that one cyt *c* is essential for ETC function and parasite viability, while the second, more divergent protein has unusual structural and biochemical properties and is not required for growth of blood-stage parasites. This work elucidates key biochemical properties and evolutionary differences in the mitochondrial ETC of malaria parasites.

Malaria is a devastating human disease that remains a pressing global health challenge. Symptoms of malaria are caused by red blood cell (RBC) infection by eukaryotic single-celled parasites of the genus *Plasmodium*, with most severe infections and deaths due to *Plasmodium falciparum*. RBCs are the most heme-rich cell in the human body, and heme metabolism is central to blood-stage parasite biology and therefore a potential vulnerability (1–3). Indeed, drugs that interfere or interact with heme-dependent metabolism in parasites have historically provided potent antimalarial therapies, including chloroquine, atovaquone, and artemisinin (4). During their 48-h life cycle after RBC invasion, malaria parasites internalize and proteolytically degrade up to 80% of red cell hemoglobin (5). This massive catabolic process liberates prodigious amounts of labile heme that is detoxified via biomineralization into inert crystalline hemozoin within the acidic parasite digestive vacuole (Fig. 1). 4-Aminoquinoline drugs such as chloroquine have potent antimalarial activity via their consensus mechanism of blocking hemozoin formation that results in the accumulation of toxic labile heme (4, 6).

P. falciparum also requires heme as an essential metabolic cofactor, although cellular uses are sparsely studied and surprisingly few heme proteins are annotated in the parasite genome (2, 3). Parasites retain a mitochondrial electron transport chain (ETC) with heme-dependent cytochromes *b* and c_1 in complex III, cytochrome (cyt) *c* as a mobile electron carrier between complexes III and IV, and the heme A-containing CoxI subunit of complex IV (Fig. 1). Complex III binds reduced ubiquinol, oxidizes it to ubiquinone, and couples sequential electron transport via cyt *b*, Rieske 2Fe–2S, cyt c_1, cyt *c*, and complex IV to proton translocation that polarizes the inner mitochondrial membrane, through a reaction series called the Q cycle (7).

ETC function is essential for parasite viability, and drugs such as atovaquone or endochin-like quinolones (ELQs) that block ubiquinone binding to cyt *b* are lethal to *P. falciparum* (8, 9). However, parasites have redundant mechanisms to polarize the mitochondrial membrane (10), and ATP synthase is dispensable for blood-stage parasites (11), which rely on glycolysis rather than oxidative phosphorylation for ATP synthesis (12, 13). Thus, the sole essential function of the mitochondrial ETC during RBC infection is thought to be oxidative recycling of ubiquinone (10). Indeed, exogenous decyl-ubiquinone (dQ) is sufficient to rescue parasites from the lethal effects of atovaquone (14) or loss of

Preprint server: https://www.biorxiv.org/content/10.1101/2023.01.23.525242v1

Author contributions: T.J.E.-S., R.G.M, and P.A.S. designed research; T.J.E.-S., H.W., R.G.M., S.-a.N., A.E.G.-G., P.E.V., Y.J.-A., A.M.B., and F.G.W. performed research; T.J.E.-S., H.W., R.G.M., S.-a.N., A.E.G.-G., P.E.V., Y.J.-A., A.M.B., F.G.W., J.A.W., M.T.K., C.P.H., and P.A.S. analyzed data; and T.J.E.-S., H.W., and P.A.S. wrote the paper.

The authors declare no competing interest.

This article is a PNAS Direct Submission.

[1]T.J.E.-S., H.W. and R.G.M. contributed equally to this work.

[2]To whom correspondence may be addressed. Email: p.sigala@biochem.utah.edu.

This article contains supporting information online at https://www.pnas.org/lookup/suppl/doi:10.1073/pnas.2301047120/-/DCSupplemental.

Published May 1, 2023.

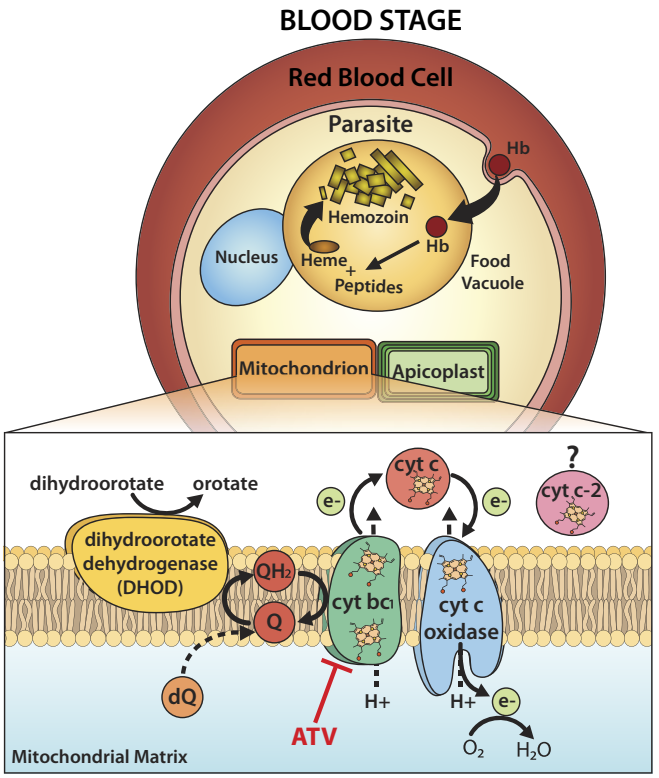

Fig. 1. Schematic model of heme metabolism during blood-stage infection by a *P. falciparum* parasite, focusing on the critical roles for heme as an electron transfer cofactor in the mitochondrial respiratory chain. Question mark indicates uncertainty in the function of the divergent cyt *c*-2 homolog. ATV = atovaquone, Q = ubiquinone, QH_2 = ubiquinol, dQ = decyl-ubiquinone. Image credit: Megan Okada, University of Utah, UT.

the Rieske Fe–S protein (15). Although multiple mitochondrial dehydrogenases require ubiquinone as an electron acceptor, dihydroorotate dehydrogenase (DHOD) appears to be the most critical of these enzymes since heterologous expression of ubiquinone-independent yeast DHOD rescues *P. falciparum* from atovaquone or ELQ toxicity (9, 10). The special vulnerability of heme-dependent mitochondrial functions for targeting *P. falciparum* in multiple developmental stages was emphasized by a recent high-throughput drug screen that identified mitochondrial ETC and DHOD inhibitors as the largest class of compounds showing dual efficacy against blood- and liver-stage parasites (16).

Heme-dependent cytochromes of complexes III and IV are key components of the ETC, but their functions have not been directly studied. *P. falciparum* also curiously encodes two divergent cyt *c* homologs, and their functions and essentiality for parasite growth remain uncertain. *C*-type cytochromes like cyt *c* and the related cyt c_1 covalently bind heme via conserved Cys residues that form stable thioether bonds to the side-chain vinyl groups of heme, in contrast to other proteins that exclusively bind heme via noncovalent interactions. Covalent heme binding depends on the additional mitochondrial protein, holocytochrome *c* synthase (HCCS) (17). Although humans encode a single bifunctional HCCS protein that attaches heme to both cyt *c* and c_1, *Plasmodium* encodes two HCCS homologs thought to be specific for hemylation of cyt *c* (HCCS) or cyt c_1 (HCC_1S) but whose specificities remain untested (2, 18).

To test and distinguish the functional importance of *c*-type cytochromes for *P. falciparum*, we used CRISPR/Cas9 to tag cyt c_1 and both cyt *c* homologs for conditional knockdown. These studies reveal that cyt c_1 (PF3D7_1462700) and the more conserved cyt *c* homolog (PF3D7_1404100) are essential for ETC function and parasite viability. The divergent cyt *c*-2 (PF3D7_1311700), however, is dispensable for blood-stage parasite growth. Despite their substantial sequence divergence, both cyt *c* homologs are selectively hemylated by the parasite HCCS (PF3D7_1224600) but not HCC_1S (PF3D7_1203600). Finally, biophysical studies strongly suggest that the divergent cyt *c*-2 binds ferric heme in an unusual penta- rather than hexa-coordinate ligation environment, despite conservation of axial His and Met ligands, and has a binding pocket that exposes heme to exogenous ligands. This work provides a direct functional dissection of mitochondrial cytochromes in malaria parasites, identifies *c*-type cytochrome hemylation as a potential target for antimalarial drug discovery, and uncovers a divergent eukaryotic cytochrome *c* (*c*-2) with highly unusual molecular adaptations and physical properties.

Results

Mitochondrial Localization of *c*-Type Cytochromes and Holocytochrome *c* Synthases. Because localization data have not previously been reported for the annotated *P. falciparum* *c*-type cytochromes or holocytochrome *c* synthases, we tested the mitochondrial targeting of these proteins by live-cell microscopy. We created Dd2 *P. falciparum* lines that episomally expressed cyt *c*, cyt *c*-2, cyt c_1, HCCS, or HCC_1S with a C-terminal GFP tag. For all the five proteins, the fluorescence signal observed for GFP colocalized with signal for MitoTracker Red (Fig. 2 and *SI Appendix*, Fig. S1), confirming mitochondrial targeting. This localization is consistent with general biochemical expectations for these proteins and with a recent proteomic study that identified cytochromes *c* and c_1 in *P. falciparum* mitochondrial extracts (19). Our studies of endogenously tagged cyt *c* and *c*-2 using immunoprecipitation/mass spectrometry and immunofluorescence also supported mitochondrial localization of these proteins (see below). Live-cell images of parasites expressing cyt c_1-GFP acquired on a higher-resolution Airyscan confocal microscope (*SI Appendix*, Fig. S2) further supported mitochondrial localization but could not distinguish suborganellar targeting to the intermembrane space (IMS), the expected localization of *c*-type cytochromes and HCCS homologs.

Divergent Sequence Features of *P. falciparum* Cytochrome *c* Homologs. We first focused on the two unusually divergent cyt *c* homologs in *P. falciparum*. Cytochrome *c* is one of the most highly conserved proteins in eukaryotes due to its centrality in mitochondrial ETC function and cellular metabolism. Indeed, its sequence variation among distinct organisms has served as a paradigm for understanding protein evolution and as a biomarker for establishing phylogenetic relationships (20–22). To assess whether the two annotated *P. falciparum* cyt *c* homologs contain the expected sequence features for conserved function within the mitochondrial ETC, we aligned the sequences of both proteins and human cytochrome *c* (Uniprot P99999).

The primary sequence of *P. falciparum* cyt *c* (PF3D7_1404100) contains a short, parasite-specific N-terminal extension of 11 residues but is otherwise 64% identical to human cyt *c* and retains the expected molecular signatures for a conserved role in mitochondrial electron transport (Fig. 3*A*). These features include i) the CXXCH motif comprised of the two Cys residues that form covalent thioether bonds to the vinyl side-chains of heme and the His residue that serves as an axial heme ligand (Fig. 3*B*), ii) Lys and Phe residues on a predicted α-helix that is N-terminal to the CXXCH motif and which are critical for HCCS recognition and covalent heme attachment (17, 23), iii) the C-terminal Met80 residue (human cyt *c* numbering) that serves as the second axial

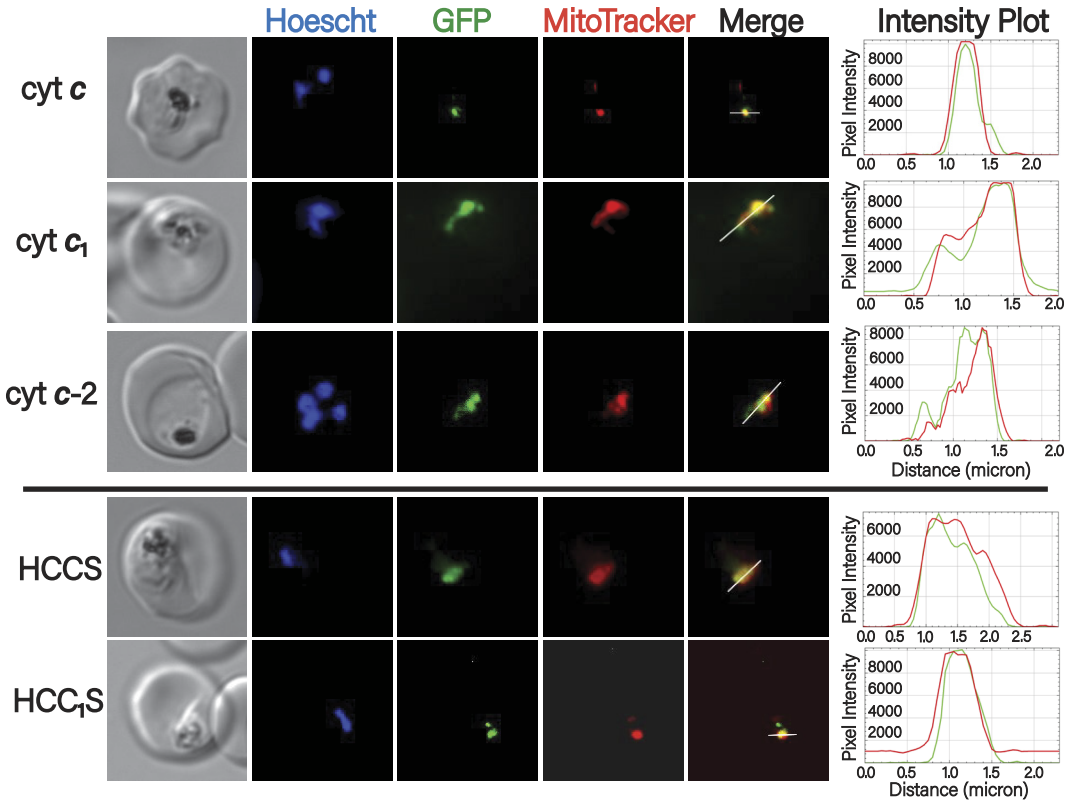

Fig. 2. Localization of *c*-type cytochromes and holocytochrome *c* synthase proteins in blood-stage parasites. Images were obtained by live epifluorescence microscopy of parasites expressing episomal second copies of each protein with a C-terminal GFP tag and stained with MitoTracker Red (mitochondrion) and Hoechst (nucleus). The intensity plot to the right of each image series displays the overlap in pixel intensity for GFP and MitoTracker Red as a function of distance along the white line in the merged image.

heme ligand (Fig. 3*B*), and iv) nearly complete identity of heme-crevice residues immediately N-terminal to Met80 (especially Lys72) that position Met80 for optimal heme coordination and mediate binding to cyt c_1 in ETC complex III (7, 20, 24). This high level of sequence conservation suggests that PF3D7_1404100 may retain canonical cyt *c* function as a mobile electron carrier in the mitochondrial ETC.

In contrast to *P. falciparum* cyt *c*, the cyt *c*-2 homolog (PF3D7_1311700) shares less than 32% identity with human cyt *c* and features extended, parasite-specific N- and C-termini as well as two short insertions (Fig. 3*A*) that further reduce overall sequence identity. This low level of sequence conservation for a eukaryotic cyt *c* homolog is highly unusual, and *P. falciparum* cyt *c*-2 is the most divergent eukaryotic cyt *c* homolog currently known (20). Cyt *c*-2 retains the key N-terminal HCCS recognition residues, the CXXCH motif, and Met80, which suggests that this protein is hemylated in the parasite mitochondrion and has the expected biaxial His/Met heme ligands. However, the heme crevice region in cyt *c*-2 has completely diverged from human and parasite cyt *c*, including loss of Lys72 and the curious insertion of a His residue upstream of Met80 (Fig. 3*A*). Mutations in this region, which is the most highly conserved sequence segment in eukaryotic cyt *c* homologs (20, 21), as well as specific introduction of a His residue, have been shown to destabilize axial coordination of heme by Met80, perturb the cyt *c* reduction potential, and weaken cyt *c* binding to ETC complex III (24–27). The total sequence divergence of the heme crevice region in *P. falciparum* cyt *c*-2 strongly suggests that this protein is likely to have an altered heme coordination environment, perturbed reduction potential, and overall physical properties that are not optimized to mediate electron transfer between ETC complexes III and IV. Based on these sequence differences, we predicted cyt *c*-2 to have a divergent function distinct from the conserved parasite cyt *c*.

Bacterial Reconstitution of cyt *c* Hemylation and Tests of Parasite HCCS Specificities. Covalent heme attachment to *c*-type cytochromes requires the IMS protein holocytochrome *c* synthase (HCCS), which binds heme and the N-terminal α-helix of cyt *c* such that the heme vinyl groups are positioned adjacent to the CXXCH of cyt *c* to accelerate stereospecific thioether bond formation (17). Both parasite cyt *c* and *c*-2 retain the N-terminal residues required for HCCS recognition and hemylation (Fig. 3*A*). Nevertheless, given the unusually high sequence divergence of cyt *c*-2, we considered it uncertain whether this protein would be hemylated by HCCS.

We tested the specificities of *P. falciparum* HCCS and HCC_1S and evaluated their ability to hemylate parasite cyt *c* and *c*-2. To do so, we cloned and recombinantly coexpressed parasite cyt *c* and *c*-2 with each HCCS homolog in *E. coli* bacteria to reconstitute holocytochrome synthesis in a heterologous in-cell model system. *E. coli* synthesizes heme but lacks cytoplasmic *c*-type cytochromes or holocytochrome *c* biogenesis machinery (28, 29). However, prior studies have shown that heterologous cytoplasmic expression of mitochondrial HCCS and cyt *c* proteins in *E. coli* is sufficient to synthesize holocytochrome *c* (30, 31). Because heme is covalently linked to cyt *c* via stable thioether bonds, the bound heme comigrates with cyt *c* protein by denaturing SDS-PAGE. After transfer to membrane, cyt *c* hemylation can be detected by exploiting the weak peroxidase activity of bound heme to catalyze luminol chemiluminescence (32). As a positive control, we performed these studies in parallel with cloned, recombinant human HCCS and cyt *c*, which have been characterized in-depth using this in-cell bacterial system (23).

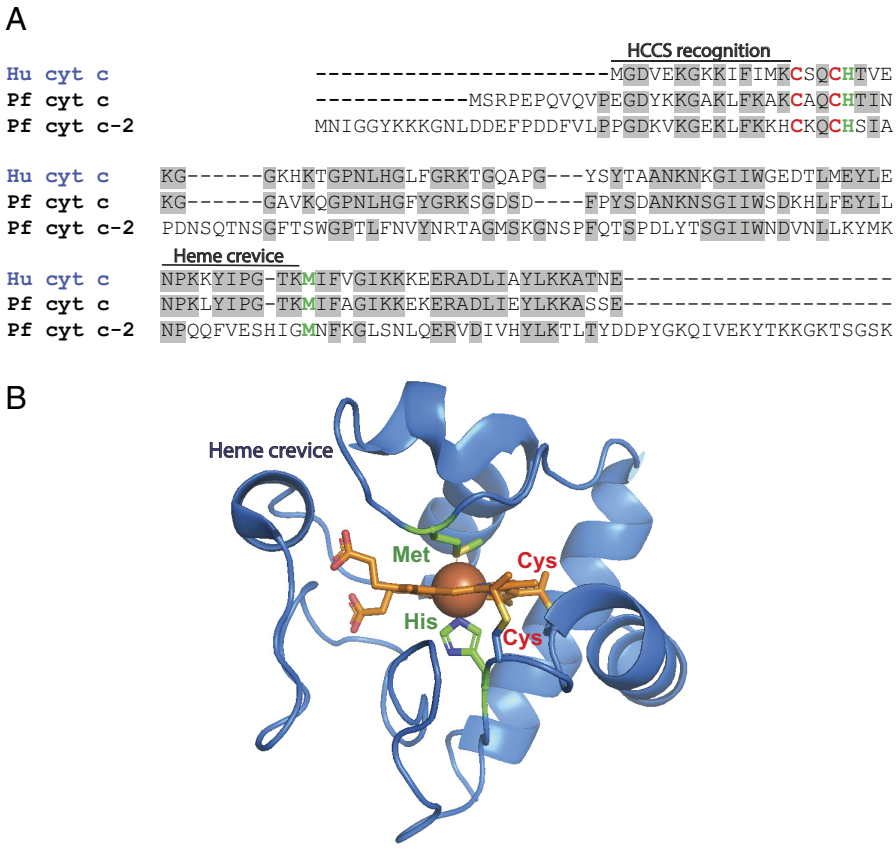

Fig. 3. Sequence and structure of cyt *c*. (*A*) Sequence comparison of human and *P. falciparum* cytochromes *c*. Identical residues are in gray. (*B*) X-ray crystallographic structure of human cyt *c* with bound heme (PDB 3NWV). Cys residues that form thioether bonds to heme are labeled in red. Conserved axial His and Met ligands are in green.

A pGEX vector encoding human HCCS with an N-terminal glutathione-S-transferase (GST) tag (23) was a gift from Robert Kranz (Washington University in St. Louis). We cloned codon-optimized genes for *P. falciparum* HCCS and HCC_1S into this pGEX vector in-frame with the N-terminal GST tag. Human cyt *c* and codon-optimized genes for *P. falciparum* cyt *c* and *c*-2 were cloned into a pET28a vector in-frame with an N-terminal hexa-histidine tag. We confirmed the expression of all HCCS and cyt *c* proteins in *E. coli* lysates by western blot analysis. Expression of each cyt *c* alone without an HCCS gave no detectable signal by chemiluminescent heme stain, confirming that cyt *c* hemylation depends on HCCS (Fig. 4). Although coexpression of human cyt *c* or malaria parasite cyt *c* or *c*-2 with human (*SI Appendix*, Fig. S3) or parasite HCCS (Fig. 4) resulted in detectable hemylation of all three cyt *c* homologs, coexpression with *P. falciparum* HCC_1S resulted in no detectable hemylation of human or parasite cyt *c* or *c*-2 (Fig. 4).

We conclude that *P. falciparum* HCCS, but not HCC_1S, is capable of hemylating parasite cyt *c* and *c*-2, consistent with predicted specificity differences for these HCCS homologs. The ability of *P. falciparum* and human HCCS to promiscuously hemylate cyt *c* homologs from both organisms suggests conserved mechanisms for substrate recognition and heme attachment by these proteins despite their phylogenetic divergence. Coexpression of *P. falciparum* HCC_1S with parasite cyt c_1 in *E. coli* did not result in detectable cyt c_1 hemylation. However, heterologous reconstitution of mitochondrial cyt c_1 hemylation in *E. coli* has not been reported for any organism, possibly due to cyt c_1 misfolding in *E. coli* and/or a requirement for additional host-cell factors for cyt c_1 hemylation. Nevertheless, the inability of HCC_1S to hemylate cyt

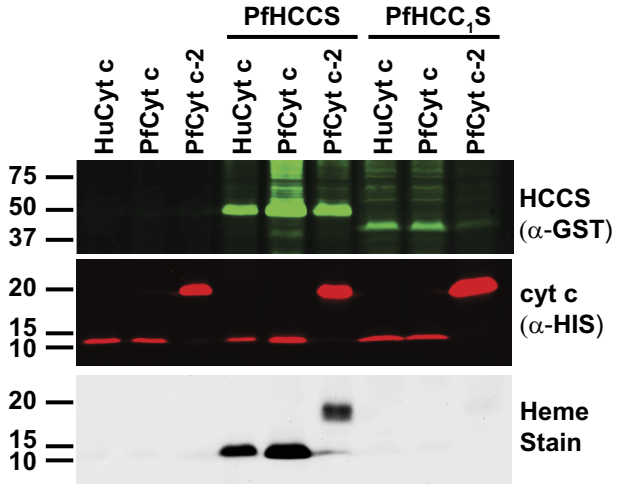

Fig. 4. Reconstitution of cyt *c* hemylation in *E. coli*. Each protein was expressed as an N-terminal fusion with GST (HCCS or HCC_1S) or His_6 (cyt *c* or *c*-2). Bacterial lysates were fractionated by SDS-PAGE and transferred to nitrocellulose membrane, which was probed with α-GST and α-His-tag antibodies. Bound heme was detected by chemiluminescent heme stain.

c is consistent with a selective role in cyt c_1 biogenesis in parasites, which we are now testing.

Optical and EPR Spectroscopy of cyt *c* Homologs Reveal Differences in Axial Heme Coordination. To assess similarities and differences in the axial heme-coordination states of human cyt *c* and *P. falciparum* cyt *c* and *c*-2, we purified these proteins from

E. coli lysates using Ni-NTA and size-exclusion chromatography (SEC) and obtained UV-vis absorbance spectra of the oxidized and reduced proteins. All the three proteins eluted from the SEC column as a single dominant peak at the expected retention time for a globular monomer (*SI Appendix*, Fig. S4). Spectra of oxidized, ferric (Fe^{3+}) human and *P. falciparum* cyt *c* were nearly identical (Fig. 5 *A* and *B*) and displayed a Soret peak centered at 410 to 412 nm and a weaker, broad transition at 535 nm that is characteristic of biaxial His/Met heme coordination in a low-spin complex (33, 34). Reduction by sodium dithionite to the ferrous (Fe^{2+}) state red-shifted the Soret peak to 417 nm for both proteins, which also displayed prominent α,β-peaks at ~520 and 550 nm (Fig. 5 *A* and *B*), as expected for a hexacoordinate complex (25). The strong spectral similarity between these two proteins is consistent with their high (~60%) sequence identity (Fig. 3*A*).

In contrast to human and parasite cyt *c*, the spectrum of oxidized, ferric *P. falciparum* cyt *c*-2 displayed a Soret peak at 408 nm, lacked the broad peak centered at 535 nm, and instead featured a weak transition at 602 nm (Fig. 5*C*). These spectral features suggest that heme is bound in a pentacoordinate, high-spin state with only one axial ligand (33, 34). These unusual properties are consistent with the high sequence divergence in the heme crevice region of cyt *c*-2 compared to human and parasite cyt *c* (Fig. 3*A*) and the expectation based on prior cyt *c* studies that heme crevice mutations perturb the positioning of Met80 (human numbering) and destabilize its coordination of heme (24, 25).

To further test the provisional conclusion that ferric cyt *c*-2 has only one stable axial ligand, we next probed whether this protein could bind exogenous small molecules as a second axial ligand. Incubation of cyt *c*-2 with a stoichiometric excess of imidazole (which mimics the His side-chain) shifted the UV-vis absorbance spectrum to resemble that of ferric human or parasite cyt *c*, including a shifted Soret peak at 411 nm, the loss of a peak at 602 nm, and appearance of a broad transition centered at 536 nm, indicative of two axial ligands (Fig. 5*C*). We observed a similar spectral shift in the presence of hydrogen peroxide (*SI Appendix*, Fig. S5). These spectral changes with exogenous ligands support a structural model that ferric cyt *c*-2 maintains axial His coordination of heme but lacks Met80 ligation (despite retaining Met80) due to structural perturbations from sequence divergence in the heme crevice residues that create an open pocket capable of binding imidazole or hydrogen peroxide as a second axial ligand.

Reduction of cyt *c*-2 with 1 mM sodium dithionite shifted the Soret peak to 418 nm and resulted in α,β-peaks at 528 and 553 nm (Fig. 5*C*), similar to ferrous human and *P. falciparum* cyt *c* and as expected for biaxial His/Met coordination of heme. The spectrum of reduced cyt *c*-2, however, rapidly reverted over several minutes to that observed for the oxidized ferric state (Fig. 5*D*). This behavior contrasted with parasite cyt *c*, which remained stably reduced over a similar timescale (*SI Appendix*, Fig. S6). This observation suggests that the heme pocket of cyt *c*-2 is more accessible to oxidation by atmospheric oxygen than that of parasite cyt *c*, consistent with altered structure and the possibility of enhanced flexibility in the heme crevice region of cyt *c*-2 due to sequence divergence.

To test and define differences in heme coordination structures and spin states of *P. falciparum* cyt *c* and *c*-2, we acquired low-temperature electron paramagnetic resonance (EPR) spectra of the oxidized proteins at 10K. The EPR spectrum of

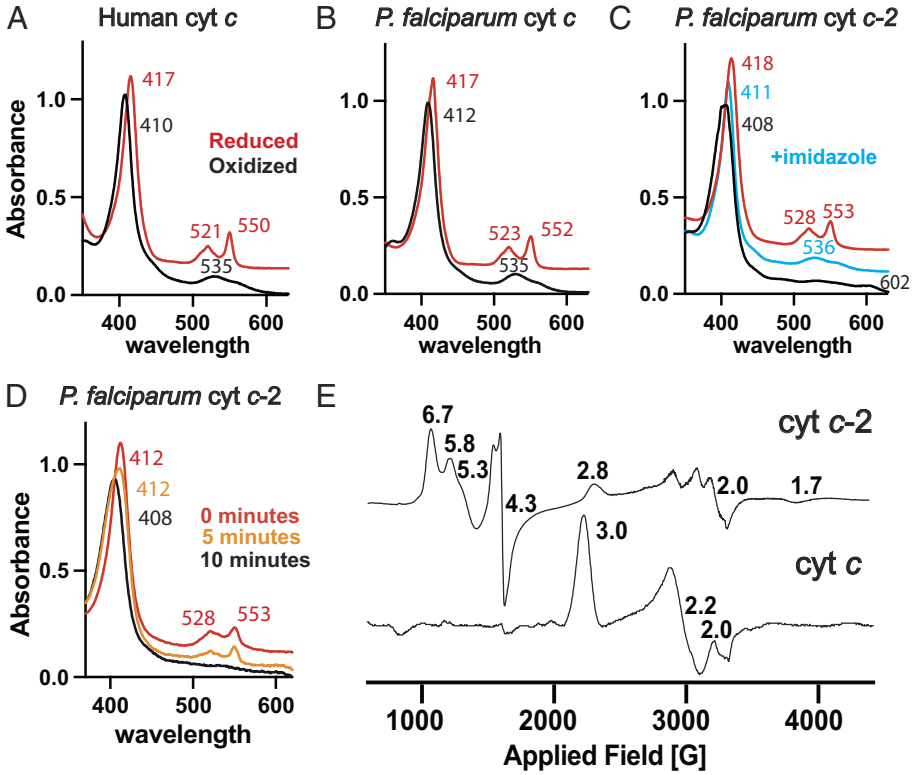

Fig. 5. Optical and EPR spectroscopy of cyt *c* homologs. UV-vis absorbance spectra of human cyt *c* (*A*) and *P. falciparum* cyt *c* (*B*) and cyt *c*-2 (*C*). Oxidized and reduced spectra were obtained in 1 mM ammonium persulfate or sodium dithionite, respectively, with 8 to 12 μM protein in phosphate-buffered saline (137 mM NaCl, 2.7 mM KCl, 4.3 mM Na_2HPO_4, 1.47 mM KH_2PO_4, pH 7.4). Spectra were normalized to the Soret peak and offset vertically to avoid overlap. For (*C*), 1 mM imidazole was added to the protein solution. (*D*) Time-dependent UV-vis absorbance spectra of parasite cyt *c*-2 after addition of sodium dithionite reducing agent. (*E*) Low-temperature EPR spectra of oxidized *P. falciparum* cyt *c* and *c*-2 acquired at 10 K. EPR g values appear above major features.

parasite cyt *c* was very similar to previously published spectra for human and yeast cyt *c* (33, 35, 36), with clear signals at g values of 3.0 and 2.2 indicative of a low-spin iron center and as expected for hexacoordinate His/Met ligation (Fig. 5*E*). This similarity is consistent with the high sequence identity and very similar UV-vis absorbance spectra of these proteins (Fig. 5 *A* and *B*).

The EPR spectrum of *P. falciparum* cyt *c*-2, however, differed substantially from human and parasite cyt *c*, with major features at g values of 6.7, 5.8, 5.3, 4.3, 2.8, and 2.0 (Fig. 5*E* and *SI Appendix*, Fig. S7). This spectrum indicates a predominant population of a high-spin heme center that is consistent with the presence of a single axial ligand, as suggested by the UV-vis absorbance spectrum. These high-spin features are similar to those reported for the H18M mutant of human cyt *c*, which was also proposed to have a single axial ligand (33). The cyt *c*-2 signals at g values of 2.8 and 2.0, however, indicate the presence of a minor low-spin population that may reflect metal contamination in the sample and/or a minor population of either hexacoordinate cyt *c*-2 with biaxial His/Met ligation or a low-lying excited state with pentacoordinate geometry.

X-Ray Crystallographic Structure of cyt *c*-2 Domain-Swapped Dimer. To better understand the structural features and unusual axial heme environment of cyt *c*-2, we determined the X-ray crystallographic structure of this protein. Sparse-matrix crystallization screens resulted in several crystals at pH 5.5 that diffracted well, and experimental phase determination enabled structure determination and refinement of a 2.3 Å-resolution structure (*SI Appendix*, Table S1). Although cyt *c*-2 is predominantly monomeric in solution at pH 7.5 (*SI Appendix*, Fig. S4), the crystal structures revealed a domain-swapped dimer (DSD) in which the C-terminal α-helix of each monomer had exchanged positions with each other to bind the neighboring subunit (Fig. 6*A*). This dimeric conformation has been observed for yeast and mammalian cyt *c* under conditions containing ethanol or detergents (37, 38). All conditions that resulted in parasite cyt *c*-2 crystals contained polyethylene glycol (PEG), and crystals formed slowly over several weeks, which may have favored crystallization of the dimeric state. Despite extensive screening, including conditions without PEG or alcohols, we were unable to crystallize a monomeric form of cyt *c*-2. These observations suggest that cyt *c*-2 has local structural heterogeneity, perhaps in the heme crevice

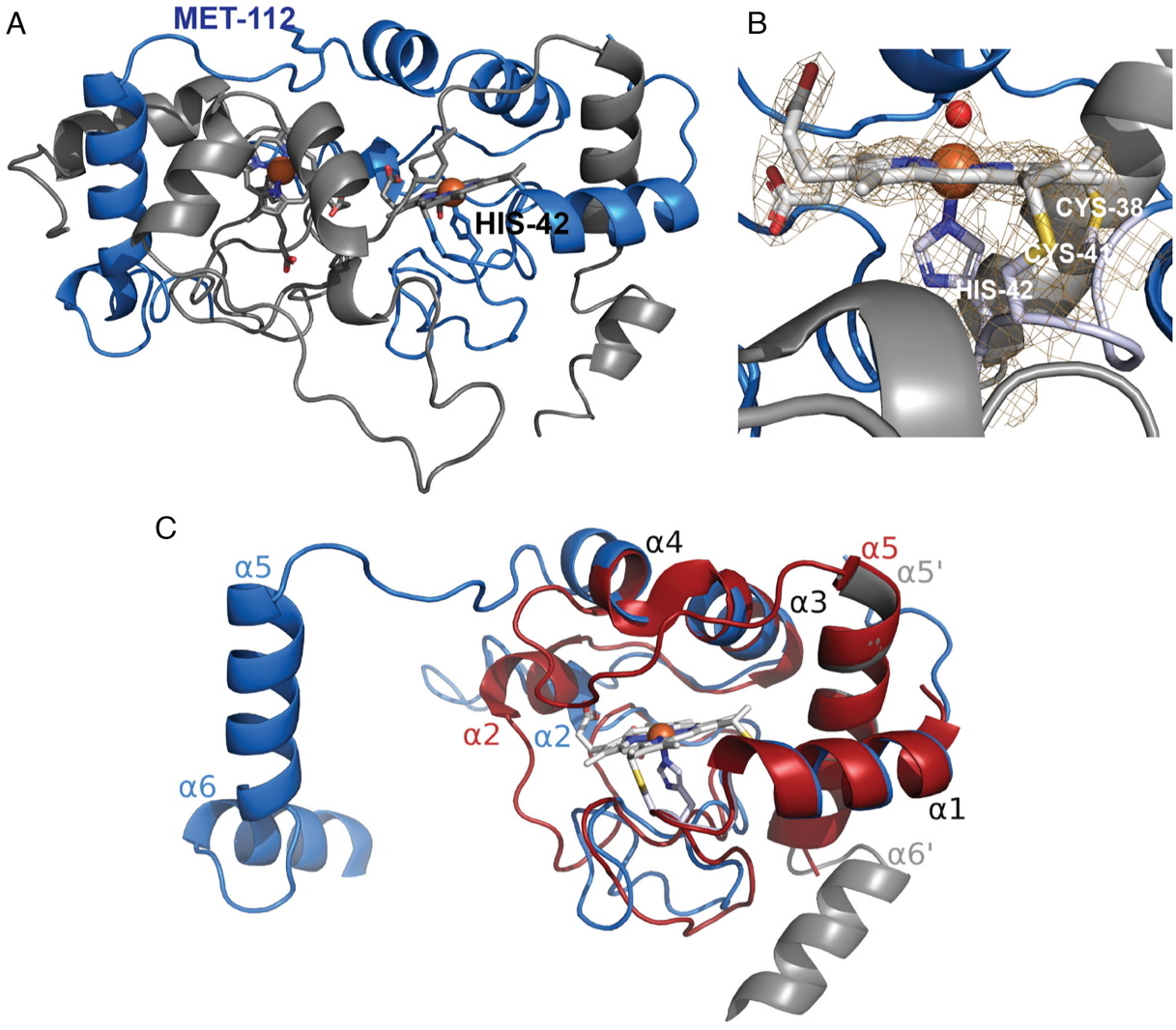

Fig. 6. X-ray crystallographic structure of *P. falciparum* cyt *c*-2. (*A*) 2.3 Å-resolution structure of the domain-swapped dimer (PDB 7TXE), with the two subunits found within the unit cell in blue and gray and His42 and Met112 sidechains shown for one subunit. (*B*) Active site of one subunit showing bound heme, axial coordination by His42, thioether bonds to Cys41 and Cys38, and 2 $|F_o|-|F_c|$ electron-density map (dark orange mesh) contoured at 1.6 σ and showing density for ordered water molecule (red sphere) positioned for axial ligation of heme, in place of Met112. (*C*) Structural backbone alignment (rmsd = 2.04 Å) of blue subunit from cyt *c*-2 domain-swapped dimer (PDB 7TXE), WT human cyt *c* (red, PDB 3ZCF), and the C-terminal helices (α5′ and α6′) of the second subunit of the cyt *c*-2 dimer (gray). Data collection and refinement statistics are in *SI Appendix*, Table S1.

region, that disfavors crystallization of the monomer and leads instead to slow crystallization of the DSD.

Despite differences from the solution state, the cyt *c*-2 dimer provided important insights into key structural features of this protein. Despite its unusually high sequence divergence, cyt *c*-2 retains an overall fold typical of eukaryotic cyt *c* proteins (37), including structural similarity in the positions of α-helices 1, 3, and 5 (21). Our structure confirmed the presence of bound heme tethered within the binding pocket by covalent thioether bonds and axial His ligation by the conserved CXXCH motif residues (Fig. 6*B*). Reciprocal swapping of C-terminal helices mispositioned the conserved Met112 (corresponding to human Met80), disrupting its ability to coordinate the iron of bound heme. Instead, we observed electron density above the iron suggestive of axial coordination by a water molecule, as observed in other cyt *c* DSD structures (37). We also noted several points of structural divergence. First, the second α-helix and residues immediately preceding it are not structurally conserved and adopt a more open conformation that increases the solvent exposure to heme. Second, the N- and C-termini of cyt *c*-2, which contain sequence extensions absent in human cyt *c* (Fig. 3*A*), adopt random-coil and α-helical conformations, respectively (Fig. 6*A*). Finally, sequence divergence in cyt *c*-2 that is N-terminal to Met112, including loss of the conserved PGTK sequence found in human and *P. falciparum* cyt *c* and insertion of an unusual His residue (Fig. 3*A*), results in a longer α-helix 4 relative to human cyt *c* (Fig. 6*C*). This secondary-structure extension in cyt *c*-2 and/or introduction of a proximal His may disfavor coordination of heme by Met112 and thus increase local structural heterogeneity in this region that enhances solvent access to heme and disfavors crystallization as a monomer. We have ongoing studies to test and understand the contribution of these sequence changes in the cyt *c*-2 heme crevice to the unusual biophysical properties of this protein.

Proteomic Analysis of Parasite cyt *c* and *c*-2 Interactions. To identify similarities and differences in protein interaction partners for parasite cyt *c* and *c*-2 that might clarify their functions, we immunoprecipitated (IP) each endogenously tagged protein and used tryptic digest followed by liquid chromatography-tandem mass spectrometry to identify coassociating proteins. For these experiments, we used CRISPR/Cas9 to introduce a C-terminal HA tag at the endogenous locus for each protein (described below) as an affinity handle for α-HA IP and used untagged parental Dd2 parasites as a negative control. Both cytochromes selectively co-purified with a range of cellular proteins, including many mitochondrial matrix and IMS proteins (*SI Appendix*, Fig. S8 and Dataset S1). Because our microscopy data indicated nearly exclusive localization of these proteins to mitochondria (Fig. 2), we focused our analysis on enriched protein interactors targeted to this organelle. Detected mitochondrial proteins included known subunits of the ETC respiratory complexes, and over 60% (23 of 36) of these interacting proteins were identified in both samples (Fig. 7). These results are consistent with the expected IMS localization of both proteins and suggest similar overall protein–protein interactions. Modest differences were observed in the copurifying proteins, but these differences did not strongly differentiate their functions.

Curiously, the kelch-13 protein (PF3D7_1343700) was selectively identified in pull-downs of both cytochromes. This protein is thought to function in the pathway of hemoglobin import into the digestive vacuole, and mutations in its propeller domain underpin parasite resistance to artemisinin (39, 40). Recent work has suggested that kelch-13 can localize to mitochondria and pull down with a variety of mitochondrial proteins, with these interactions

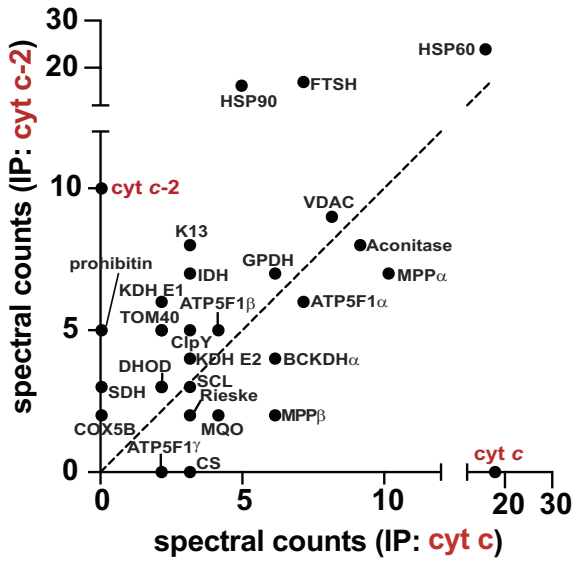

Fig. 7. IP/MS studies of protein–protein interactions for blood-stage *P. falciparum* cyt *c* and *c*-2. Bait proteins were immunoprecipitated by anti-HA-tag pull-down, and associated proteins were identified by tryptic digest and tandem mass spectrometry. Spectral counts of detected mitochondrial proteins are shown for each IP sample. None of the detected proteins were identified by anti-HA-tag IP of parental Dd2 parasites, except for HSP60 which was enriched >2-fold relative to Dd2. The dashed line has a slope of one. Source data for mitochondrial and all detected proteins are given in Dataset S1.

appearing to increase upon artemisinin treatment (41). The physical determinants and functional consequences of these associations remain uncertain. Our observation is consistent with this prior work, although the interactions that underpin direct or indirect association of cyt *c* and *c*-2 with kelch-13 remain undefined.

Critical Tests of *c*-Type Cytochrome Importance for Blood-Stage Parasites. The strong sequence conservation and similar physical properties between *P. falciparum* and human cyt *c* suggest that this parasite homolog (PF3D7_1404100) retains a conserved, essential function in the mitochondrial ETC. Indeed, recent genome-wide knockout studies in both rodent and human parasites indicated that this gene is refractory to disruption (42, 43). The divergent sequence and unusual physical properties of *P. falciparum* cyt *c*-2 (PF3D7_1311700), however, seem incompatible with a canonical ETC role and raise substantial uncertainty on its essentiality for blood-stage parasites. Recent genome-wide knockout studies have also given conflicting results for this gene, which was reported to be essential for *P. falciparum* human parasites but fully dispensable for *P. berghei* rodent parasites (42, 43).

To directly test the essentiality of each cyt *c* homolog for blood-stage *P. falciparum* growth and viability, we used CRISPR/Cas9 to tag the endogenous genomic locus for cyt *c*, cyt *c*-2, and cyt c_1 in both Dd2 and NF54 parasites to encode a C-terminal HA-FLAG epitope tag fusion and the aptamer/TetR-DOZI system (44). In this knockdown (KD) system, protein expression is enabled in the presence of anhydrotetracycline (aTc) but tightly repressed after aTc washout. Correct and complete integration into the target genomic locus was confirmed for all the three genes by PCR analysis of Dd2 and NF54 parasites and by southern blot for editing cyt *c*-2 in Dd2 parasites (*SI Appendix*, Fig. S9). Immunofluorescence microscopy experiments confirmed that all the three endogenously tagged cytochromes colocalized with mitochondrial HSP60 (*SI Appendix*, Fig. S10). Expression of each tagged protein was detected by anti-HA-tag western blot in +aTc conditions, but these proteins were nearly undetectable after 3 d of growth in -aTc conditions, indicating robust knockdown (Fig. 8 *A*–*C*).

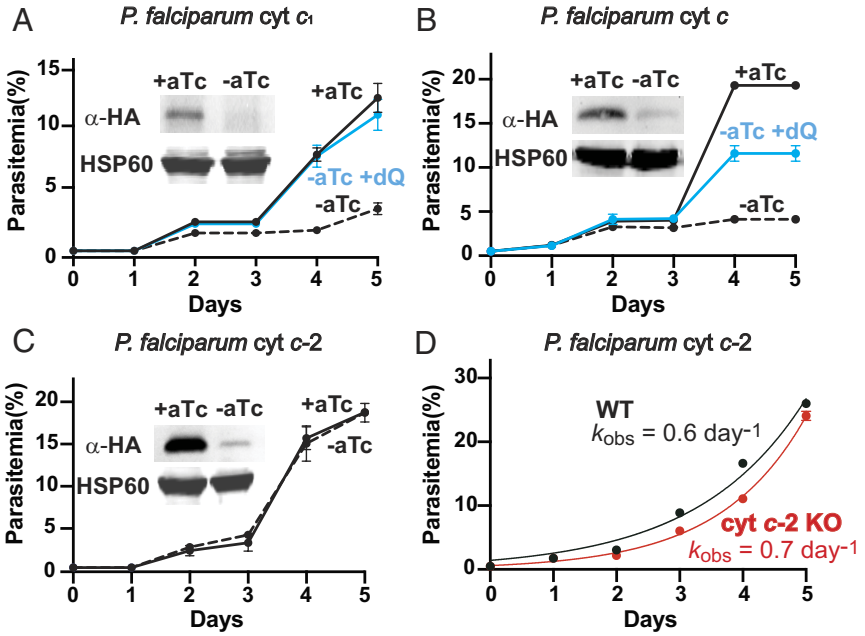

Fig. 8. Functional tests of contributions by cyt *c*-2, and c_1 to blood-stage parasite growth. Synchronous growth assays of Dd2 parasites tagged with the aptamer/TetR–DOZI cassette for inducible knockdown of cyt c_1 (*A*), cyt *c* (*B*), and cyt *c*-2 (*C*), in the presence or absence of 0.5 μM anhydrotetracycline (aTc) and 15 μM decyl-ubiquinone (dQ). Insets are α-HA and α-HSP60 western blots of parasites lysates harvested on day 3 of the continuous growth assay. Densitometry analysis indicated ≥85% reduction in protein levels for all the three cytochromes relative to mitochondrial HSP60. Uncropped western blot images are included in *SI Appendix*, Fig. S11. (*D*) Asynchronous growth assay of WT or cyt *c*-2 knockout (KO) NF54 parasites. Data were fit to an exponential growth equation to determine observed rate constants (k_{obs}). For all growth assays, data points and error bars are the mean and SD of biological triplicates.

All tagged parasites grew normally in synchronous growth assays in the presence of aTc. Washout of aTc, however, resulted in a strong growth defect after 3 d for Dd2 and NF54 parasites containing tagged cyt *c* and c_1 genes (Fig. 8 *A* and *B* and *SI Appendix*, Fig. S12). Blood smear analysis of these cultures revealed widespread parasite death upon aTc washout (*SI Appendix*, Fig. S13). In contrast, aTc washout had no detectable impact on the growth of Dd2 or NF54 cyt *c*-2 KD parasites (Fig. 8*C* and *SI Appendix*, Fig. S12), suggesting that this homolog is not essential for the growth of blood-stage *P. falciparum*. To further test this conclusion and to rule out an alternative explanation that KD of cyt *c*-2 is insufficiently stringent to observe a growth phenotype, we stably disrupted the cyt *c*-2 gene in NF54 parasites to create a knockout (KO) line (*SI Appendix*, Fig. S9). The KO parasites grew very similar to parental WT parasites, with a nearly identical rate constant for asynchronous exponential growth (Fig. 8*D*). This similarity strongly supports the conclusion that the divergent cyt *c*-2 is fully dispensable for blood-stage parasite growth.

The prevailing paradigm posits that oxidative recycling of ubiquinone is the sole essential function of the ETC in blood-stage parasites (10). In direct support of this model, we observed that exogenous addition of oxidized decyl-ubiquinone rescued growth of Dd2 parasites from KD of cyt *c* and c_1 in -aTc conditions (Fig. 8 *A* and *B*). To further test and extend this conclusion, we asked whether KD of cyt *c* or c_1 sensitized parasites to mitochondrial depolarization by proguanil. This drug targets a secondary pathway in parasites for maintaining mitochondrial transmembrane potential that only becomes essential upon ETC dysfunction (10, 45). Growth of cyt *c* or c_1 KD parasites cultured in +aTc conditions was unaffected by 1 μM proguanil, as expected for an active ETC. However, when 1 μM proguanil was combined with -aTc conditions, decyl-ubiquinone was unable to rescue parasites from lethal growth defect on day four (Fig. 9 *A* and *B*). Analysis of parasites on day three of these growth assays by fluorescence microscopy revealed that 1 μM proguanil selectively resulted in dispersed rather than focal staining by MitoTracker Red in cyt *c* or c_1 KD parasites grown in -aTc conditions (Fig. 9 *C* and *D* and *SI Appendix*, Fig. S14), which is indicative of mitochondrial depolarization (10, 15). These observations strongly support our conclusion that loss of cyt *c* or c_1 results in lethal ETC dysfunction that sensitizes parasites to mitochondrial depolarization when treated with proguanil.

Discussion

The mitochondrial ETC of *Plasmodium* parasites has been the subject of intense drug development efforts over the past several decades to block parasite growth in blood, liver, and mosquito stages (9, 10, 16, 46–49). Nevertheless, key ETC functions have remained uncertain and puzzling. Indeed, many mitochondrial proteins in *Plasmodium* have divergent sequence features and/or are specific to apicomplexan parasites (15, 19, 50–52). In addition, the activity and essentiality of distinct ETC components vary across different parasite developmental stages with the shifting nutritional availability and energy requirements of *Plasmodium* in discrete host environments (1, 11, 13, 19, 49, 53, 54). This functional complexity and the sparsity of direct molecular studies of complexes III and IV have left critical gaps in our basic understanding of parasite ETC function and evolution (3, 55, 56).

Direct Tests of Mitochondrial Cytochrome Functions. We have carried out direct tests of ETC cytochrome functions in *P. falciparum*, focusing on the nuclear-encoded *c*-type cytochromes. Our results indicate that cyt c_1 and the more conserved cyt *c* (PF3D7_1404100) are essential for viability of blood-stage *P. falciparum*, while the divergent cyt *c*-2 (PF3D7_1311700) is dispensable in this stage.

The ability of dQ to rescue parasites from loss of cyt *c* or c_1 provides direct experimental support to the general paradigm, based predominantly on inhibitor studies of cyt *b*, that the

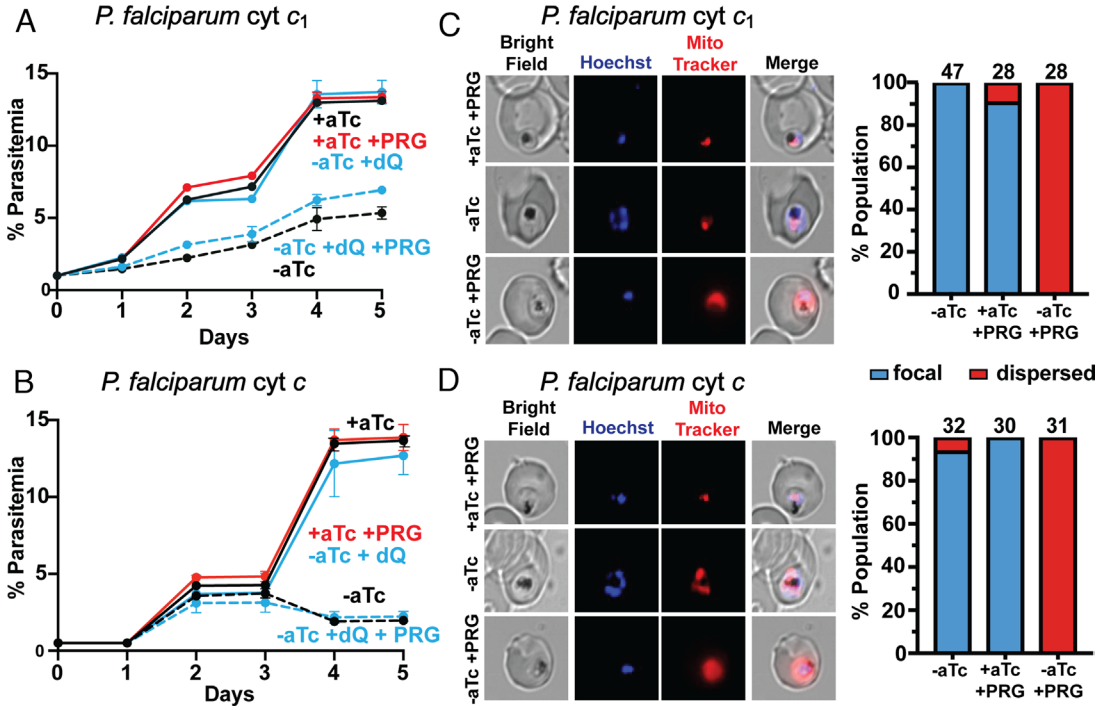

Fig. 9. Loss of ETC cytochromes sensitizes parasites to proguanil. Synchronous growth assays of Dd2 parasites tagged with the aptamer/TetR–DOZI cassette for inducible knockdown of cyt c_1 (*A*) and cyt *c* (*B*) in the presence or absence of 0.5 μM anhydrotetracycline (aTc), 1 μM proguanil (PRG), and/or 15 μM decylubiquinone (dQ). Data points and error bars are the mean ±SD of biological triplicates. Fluorescence microscopy images of live cyt c_1 (*C*) or cyt *c* (*D*) aptamer/TetR–DOZI Dd2 parasites cultured for 3 d ±aTc and ±1 μM proguanil and stained with Hoechst or MitoTracker Red (10 nM). The parasites were imaged in biological duplicate experiments to count 28 to 47 total parasites, score MitoTracker staining as focal or dispersed, and depict the percentage of the total population under each condition displaying the indicated mitochondrial phenotype.

essential ETC function in blood-stage parasites is oxidative recycling of ubiquinone to support essential dehydrogenase activity, especially dihydroorotate dehydrogenase (Fig. 1) (9, 10, 14). Prior work has also suggested that parasites have a secondary and redundant pathway for polarizing the inner mitochondrial membrane that is independent of proton translocation by complexes III and IV and can be blocked by low-dose proguanil (10, 45). In support of this model, we observed that loss of cyt *c* or c_1 and concomitant defects in ETC-mediated proton translocation did not result in mitochondrial depolarization, which only occurred upon combinatorial treatment with proguanil (Fig. 9). These results are also consistent with our prior study of the mitochondrial acyl carrier protein in *P. falciparum,* whose knockdown results in loss of the Rieske Fe–S protein required for complex III function and can be bypassed by exogenous dQ (15).

Recent proteomic studies of ETC composition in *P. falciparum* and *T. gondii* have identified the mitochondrial processing peptidase (MPP) α and β subunits as key constituents of complex III (19, 57, 58), as observed in plants (59, 60). MPP cleaves the N-terminal leader sequences of proteins imported into mitochondria and appears to be essential for *P. falciparum* (43). We observed that both parasite cyt *c* homologs pulled down with MPP subunits, with somewhat higher detection of MPP association for cyt *c* than *c*-2 (Fig. 7), consistent with complex III interactions. Whether MPP enzymatic activity requires or is independent of association with complex III is unstudied in parasites. However, our results may provide insight into this question. Loss of cyt c_1 is expected to strongly destabilize complex III, with cyt c_1 knockout resulting in >80% reduction in cyt *b* levels in yeast (61). The ability of dQ to rescue parasites from cyt c_1 knockdown (Figs. 8*A* and 9*A*) suggests that MPP activity may persist independent of complex III integrity, since dQ is not expected to bypass more general defects in MPP processing. Biochemical precedent for autonomous MPP function is provided by yeast and humans, in which MPP is a soluble matrix enzyme that functions independent of complex III (62).

Cytochrome *c* Duplication in *Plasmodium* and Comparison to Other Eukaryotes. Sequencing of the *P. falciparum* genome revealed that parasites encode two copies of cyt *c*, raising questions about the biochemical rationale for this duplication and the functional roles of the distinct paralogs (2, 51, 63). Confusion and uncertainty increased after genome-wide knockout studies gave conflicting assessments of essentiality (42, 43). Although both proteins are expressed (Figs. 8 and 9), only the conserved cyt *c* is required for *Plasmodium* ETC activity in blood-stage parasites.

Cyt *c*-2 has the most divergent sequence of any known eukaryotic cyt *c*, with functional properties that are not required for ETC activity in blood-stage parasites. These changes in a eukaryotic cyt *c* homolog are fascinating and uncommon, given stringent fitness constraints that disfavor substantial sequence divergence in cyt *c* in order to retain its essential role in mitochondrial respiration (20, 21). Indeed, the strong sequence conservation between cyt *c* from diverse eukaryotes has served as a paradigm for understanding molecular evolution, organismal phylogeny, and the relationships between natural selection and sequence variation (22, 64, 65).

Saccharomyces cerevisiae also has two copies of cyt *c*. However, their sequence identity is high (>80%), and their functions appear to be redundant since both copies must be deleted to cause full respiratory deficiency (66, 67). Cyt *c* duplication is also found throughout the phylum Apicomplexa, including *Toxoplasma* and *Babesia*, and in the closely related photosynthetic chromerid, *Vitrella brassicaformis*. These organisms are similar to *Plasmodium*, with one highly conserved homolog of cyt *c* and a second copy with sequence divergence approaching that of *P. falciparum* cyt *c*-2. *Toxoplasma* resembles *Plasmodium* in that the more conserved homolog (TGME49_219750) is essential while the more divergent

homolog (TGME49_229420) appears dispensable for tachyzoite growth in fibroblasts (68). Ancestral gene duplication, including whole-genome duplication in *S. cerevisiae* (69), can account for the multiple copies of cyt *c* in these organisms (70). Apicomplexan cyt *c* and *c*-2 may have evolved from specific duplication of an ancestral cyt *c* that occurred at or near the appearance of apicomplexan parasitism >600 Mya prior to the last common ancestor of *Vitrella, P. falciparum,* and *T. gondii* (71). Different selective pressures presumably resulted either in strong sequence conservation between both copies in yeast or in substantial divergence in Apicomplexa and *Vitrella*.

Divergent Function of *Plasmodium* Cytochrome *c*-2. The *P. falciparum* genome is highly reduced, and all genes are expected to enhance parasite fitness at some point in the *Plasmodium* life cycle and/or under specific growth conditions or stresses (63, 72, 73). Retention of the cyt *c*-2 coding sequence in parasites and conservation of its covalent heme-binding features and axial His/Met ligands thus suggest a selective pressure to preserve gene function and to resist sequence degradation, in contrast to cyt *c* pseudogenes found in humans and other organisms that acquired disabling frameshift and nonsense mutations (70, 74). What then is the molecular function of *Plasmodium* cyt *c*-2, and what fitness contributions explain its retention in the parasite genome?

Our structural and spectroscopic studies of cyt *c*-2 reveal an unusually open active site in which ferric heme is bound within a flexible pocket and stably coordinated by only a single axial ligand, His42 (Figs. 5 and 6). These structural features create a pocket above the heme into which small-molecule ligands such as imidazole can bind. Conservation of Met112 in parasite cyt *c*-2, despite not stably coordinating ferric heme, may reflect a functional role for this residue in transient interactions with heme, including key steps in hemylation by HCCS (23). Destabilization of axial heme coordination by Met112 is expected to perturb the cyt *c*-2 reduction potential. Preliminary measurements indicate a redox potential ~260 mV for parasite cyt *c*, which is very similar to human cyt *c,* but suggest a very different potential for cyt *c*-2 than expected for canonical ETC function (25, 33). Overall, cyt *c*-2 has divergent physical properties that defy a conserved function in the mitochondrial ETC, even if hemylation and mitochondrial localization are retained.

Cyt *c* in mammals and other organisms plays a second critical role in cellular apoptosis, during which cyt *c* binds cardiolipin and transiently adopts an altered conformation that destabilizes axial Met coordination and opens up the heme pocket to enhance intrinsic peroxidase activity (25, 75, 76). Our studies suggest that *P. falciparum* cyt *c*-2 has evolved constitutive physical properties that may mimic aspects of the transient conformational state adopted by canonical cyt *c* homologs during apoptosis, including disruption of heme coordination by Met and an open pocket above heme capable of binding peroxides and other ligands (*SI Appendix*, Fig. S5). Based on these features, we hypothesize that cyt *c*-2 has evolved constitutive peroxidase function that is enhanced relative to cyt *c*, which we are currently testing. This proposed function is notable, since *P. falciparum* lacks canonical heme-dependent peroxidases and catalases typically involved in antioxidant protection (2, 3). Cyt *c*-2 is dispensable for blood-stage parasites but may play a critical role in other host environments or specific growth conditions, including increased oxidative stress. Preliminary experiments, which suggest that cyt *c*-2 KO parasites are two to threefold more sensitive to artemisinin than parental NF54 parasites (*SI Appendix*, Fig. S15), support this hypothesis.

Cyt *c*-2 transcription is substantially up-regulated (~80 fold) in mosquito-stage ookinetes relative to blood-stage trophozoites (77, 78), suggesting heightened function and fitness contributions during parasite growth in the insect vector. This observation is intriguing, since oxidative mitochondrial activity and ETC flux in *Plasmodium* increase during parasite development in mosquitoes and may enhance the production of hydrogen peroxide and other reactive oxygen species as ETC by-products (11, 54, 79–83). We speculate that cyt *c*-2 may contribute to oxidative metabolism and/or stress protection in this stage, including possible impacts on parasite sensitivity to drugs such as atovaquone that target mitochondrial function during growth in mosquitoes (46, 81). We are currently testing cyt *c*-2 function during parasite infection of mosquitoes.

Materials and Methods

SI Appendix contains a full description of *Materials and Methods* in *SI Appendix, Supporting Methods*, Figs. S1 to S15 and Tables S1 and S2, the legend for Dataset S1, and *SI Appendix, SI References*.

Cloning. The genes encoding cyt *c* (PF3D7_1404100), cyt *c*-2 (PF3D7_1311700), cyt c_1 (PF3D7_1462700), HCCS (PF3D7_1224600), and HCC_1S (PF3D7_1203600) were PCR-amplified from Dd2 parasite gDNA or cDNA and cloned into pTEOE (84) in-frame with a C-terminal GFP tag, using previously published methods (15). Codon-optimized versions of these genes were cloned into pET28a (cytochromes, N-terminal His_6 tag) or pGEX ($HCCS/HCC_1S$, N-terminal GST tag) for expression in *E. coli*. CRISPR/Cas9 and double-crossover homologous recombination were used to disrupt the cyt *c*-2 gene and to tag all the three cyt genes for inducible knockdown using the aptamer/TetR-DOZI system (44). Correct sequences for all plasmids were confirmed by Sanger sequencing.

Parasite Culturing, Transfection, and Growth Assays. Experiments reported in this study were performed using *P. falciparum* parasite strains Dd2 (85) and NF54 (86). Parasite culturing, transfection, and selection were performed as previously described (87). Parasite continuous growth assays and 48-h dose–response assays were performed using biological triplicate samples as previously described (15, 88).

SDS-PAGE and Western Blot Analyses. Analysis of cyt *c* hemylation in *E. coli* was performed by coexpression of each cyt with human HCCS in BL21/DE3 bacteria, fractionation of lysates by SDS-PAGE, transfer to nitrocellulose membrane, and staining with the Prometheus™ ProSignal Femto ECL reagent. Expression of endogenous cyt *c*, cyt c_1, and cyt *c*-2 in blood-stage *P. falciparum* parasites was performed using previously described methods (15), with minor modifications.

Fluorescence Microscopy. Images of live and fixed/stained parasites were taken on DIC/brightfield, DAPI, GFP, and RFP channels using an EVOS M5000 imaging system, a Nikon widefield fluorescence microscope, or an Airyscan LSM800 confocal microscope (Carl Zeiss). Fiji/ImageJ was used to process and analyze images. Two-dimensional intensity plots were generated in Fiji/ImageJ with the "plot profile" function.

Recombinant Protein Expression and Purification. Heterologous expression and purification of hemylated cyt *c* was performed with BL21 DE3 *E. coli* cells cotransformed with pET28a (encoding human or *P. falciparum* cyt *c* or cyt *c*-2 with N-terminal His-tag) and pGEX (encoding human HCCS with N-terminal GST tag) plasmids. Hemylated cyt proteins were purified from lysates by Ni-NTA agarose affinity chromatography, SP cation-exchange chromatography, and size-exclusion chromatography, using prior methods (15) with minor modifications. Protein purity and identity were confirmed by Coomassie-stained SDS-PAGE and by LC-MS/MS.

Protein Crystallization and X-Ray Structure Determination. Crystals of *Plasmodium falciparum* cyt *c*-2 containing bound heme were grown by sitting drop vapor-diffusion method at 21 °C. Diffraction data were collected at beamlines 9 to 2 and 12 to 1 at the Stanford Synchrotron Radiation Lightsource (SSRL). Initial phases were determined by single-wavelength anomalous dispersion (SAD) phasing methods in PHENIX using the anomalous signal from the heme iron. COOT (89) and PHENIX (90) were used for model rebuilding and refinement, respectively. Protein structures were visualized and aligned in PyMOL, version 2.0 (Schrödinger, LLC). Structure factors and model coordinates were deposited in the RCSB Protein Data Bank (https://www.rcsb.org) under accession codes 7TXE (2.3 Å-resolution) and 7U2V (2.6 Å-resolution).

EPR Spectroscopy. Electron paramagnetic resonance (EPR) spectroscopy was performed at the Utah State University Department of Chemistry and Biochemistry. For perpendicular mode continuous wave (CW) X-Band EPR measurements, ~100 µL of 100 µM samples in phosphate-buffered saline (137 mM NaCl, 2.7 mM KCl, 4.3 mM Na_2HPO_4, 1.47 mM KH_2PO_4, pH 7.4) was flash frozen in 3 mm inner diameter quartz EPR tubes in liquid nitrogen. CW EPR measurements were performed on a Bruker EMX Plus EPR spectrometer (Bruker Biospin, Billerica, MA) equipped with a liquid helium cryostat operating at X-band (9.38 GHz microwave frequency) with 4,000 G sweep width, 10.0 mG modulation amplitude, and 1 mW incident microwave power. Spectra were collected at 5.6 to 5.7 K and 9.94 K and averaged over five scans.

Mass Spectrometry. Mass spectrometry experiments with parasite protein samples isolated by anti-HA-tag IP of endogenous or purification of recombinant cyt *c* or *c*-2 were performed as previously described (15, 91).

Data, Materials, and Software Availability. Atomic coordinates and structure factors for all protein structural models have been deposited in RCSB Protein Data Bank, https://www.rcsb.org (PDB ID codes 7U2V, 7TXE). All study data are included in the article and/or supporting information.

ACKNOWLEDGMENTS. We thank Seyi Falekun for help with IP/MS experiments; Megan Okada for graphical figure preparation; Robert Kranz for plasmids encoding human HCCS and cyt *c* and helpful discussions; Shelly Minteer for assistance with redox potential measurements; and Bruce Bowler, Amit Reddi, Jared Rutter, Akhil Vaidya, and Dennis Winge for helpful discussions. Research reported in this publication was supported by a Burroughs Wellcome Fund Career Award at the Scientific Interface (to P.A.S.); NIH grants R35GM133764 (to P.A.S.) and R01GM089778 (to J.A.W.); a pilot award (to P.A.S.) from the Utah Center for Iron and Heme Disorders (U54DK110858); and a seed grant (to P.A.S.) from the University of Utah Vice President for Research. P.A.S. is a Pew Biomedical Scholar, supported by The Pew Charitable Trusts. T.J.E.-S. and A.M.B. were supported by NIH training grant T32DK007115. S.-a.N. was supported by the Utah Native American Research Internship (R25HL108828) and by NIH diversity supplement R35GM133764-04S1. DNA synthesis and sequencing, fluorescence microscopy, creation of CRISPR/Cas9 reagents, recombinant protein mass spectrometry, and flow cytometry were performed using University of Utah core facilities. EPR experiments were performed at Utah State University, with instrumentation supported by NSF grant MRI-0722849. Use of the Stanford Synchrotron Radiation Lightsource is supported by the U.S. Department of Energy Contract No. DE-AC02-76SF00515 and by the NIH (P30GM133894). Fig. 1 was adapted from ref. (92).

Author affiliations: [a]Department of Biochemistry, University of Utah School of Medicine, Salt Lake City, UT 84112; [b]Department of Chemistry, University of Utah, Salt Lake City, UT 84112; and [c]Department of Biological Chemistry, University of California, Los Angeles, CA 90095

1. P. A. Sigala, D. E. Goldberg, The peculiarities and paradoxes of *Plasmodium* heme metabolism. *Annu. Rev. Microbiol.* **68**, 259–278 (2014).
2. G. G. van Dooren, A. T. Kennedy, G. I. McFadden, The use and abuse of heme in apicomplexan parasites. *Antioxid. Redox Signal.* **17**, 634–656 (2012).
3. J. Kloehn, C. R. Harding, D. Soldati-Favre, Supply and demand-heme synthesis, salvage and utilization by Apicomplexa. *FEBS J.* **288**, 382–404 (2021).
4. B. Blasco, D. Leroy, D. A. Fidock, Antimalarial drug resistance: Linking *Plasmodium falciparum* parasite biology to the clinic. *Nat. Med.* **23**, 917–928 (2017).
5. S. E. Francis, D. J. Sullivan Jr., D. E. Goldberg, Hemoglobin metabolism in the malaria parasite *Plasmodium falciparum*. *Annu. Rev. Microbiol.* **51**, 97–123 (1997).
6. D. J. Sullivan Jr., H. Matile, R. G. Ridley, D. E. Goldberg, A common mechanism for blockade of heme polymerization by antimalarial quinolines. *J. Biol. Chem.* **273**, 31103–31107 (1998).
7. Z. Zhang *et al.*, Electron transfer by domain movement in cytochrome bc1. *Nature* **392**, 677–684 (1998).
8. M. Fry, M. Pudney, Site of action of the antimalarial hydroxynaphthoquinone, 2-[trans-4-(4′-chlorophenyl) cyclohexyl]-3-hydroxy-1,4-naphthoquinone (566C80). *Biochem. Pharmacol.* **43**, 1545–1553 (1992).
9. A. Nilsen *et al.*, Quinolone-3-diarylethers: A new class of antimalarial drug. *Sci. Transl. Med.* **5**, 177ra137 (2013).
10. H. J. Painter, J. M. Morrisey, M. W. Mather, A. B. Vaidya, Specific role of mitochondrial electron transport in blood-stage *Plasmodium falciparum*. *Nature* **446**, 88–91 (2007).
11. A. Sturm, V. Mollard, A. Cozijnsen, C. D. Goodman, G. I. McFadden, Mitochondrial ATP synthase is dispensable in blood-stage *Plasmodium berghei* rodent malaria but essential in the mosquito phase. *Proc. Natl. Acad. Sci. U.S.A.* **112**, 10216–10223 (2015).
12. M. Fry, E. Webb, M. Pudney, Effect of mitochondrial inhibitors on adenosinetriphosphate levels in *Plasmodium falciparum*. *Comp. Biochem. Physiol. B* **96**, 775–782 (1990).
13. J. I. MacRae *et al.*, Mitochondrial metabolism of sexual and asexual blood stages of the malaria parasite *Plasmodium falciparum*. *BMC Biol.* **11**, 67 (2013).
14. H. J. Ke *et al.*, Variation among *Plasmodium falciparum* strains in their reliance on mitochondrial electron transport chain function. *Eukaryot. Cell* **10**, 1053–1061 (2011).
15. S. Falekun *et al.*, Divergent acyl carrier protein decouples mitochondrial Fe-S cluster biogenesis from fatty acid synthesis in malaria parasites. *Elife* **10**, e71636 (2021).
16. Y. Antonova-Koch *et al.*, Open-source discovery of chemical leads for next-generation chemoprotective antimalarials. *Science* **362**, eaat9446 (2018).
17. S. E. Babbitt, M. C. Sutherland, B. San Francisco, D. L. Mendez, R. G. Kranz, Mitochondrial cytochrome c biogenesis: No longer an enigma. *Trends Biochem. Sci.* **40**, 446–455 (2015).
18. N. Posayapisit *et al.*, Cytochrome c and c1 heme lyases are essential in *Plasmodium berghei*. *Mol. Biochem. Parasitol.* **210**, 32–36 (2016).
19. F. Evers *et al.*, Composition and stage dynamics of mitochondrial complexes in *Plasmodium falciparum*. *Nat. Commun.* **12**, 3820 (2021).
20. L. Banci, I. Bertini, A. Rosato, G. Varani, Mitochondrial cytochromes c: A comparative analysis. *J. Biol. Inorg. Chem.* **4**, 824–837 (1999).
21. S. Zaidi, M. I. Hassan, A. Islam, F. Ahmad, The role of key residues in structure, function, and stability of cytochrome-c. *Cell Mol. Life Sci.* **71**, 229–255 (2014).
22. E. Margoliash, Primary structure and evolution of cytochrome C. *Proc. Natl. Acad. Sci. U.S.A.* **50**, 672–679 (1963).
23. B. San Francisco, E. C. Bretsnyder, R. G. Kranz, Human mitochondrial holocytochrome c synthase's heme binding, maturation determinants, and complex formation with cytochrome c. *Proc. Natl. Acad. Sci. U.S.A.* **110**, E788–797 (2013).
24. L. J. McClelland, T. C. Mou, M. E. Jeakins-Cooley, S. R. Sprang, B. E. Bowler, Structure of a mitochondrial cytochrome c conformer competent for peroxidase activity. *Proc. Natl. Acad. Sci. U.S.A.* **111**, 6648–6653 (2014).
25. D. Alvarez-Paggi *et al.*, Multifunctional cytochrome c: Learning new tricks from an old dog. *Chem. Rev.* **117**, 13382–13460 (2017).
26. S. Godbole, B. E. Bowler, Effect of pH on formation of a nativelike intermediate on the unfolding pathway of a Lys 73 –> His variant of yeast iso-1-cytochrome c. *Biochemistry* **38**, 487–495 (1999).
27. T. Ying *et al.*, Tyrosine-67 in cytochrome c is a possible apoptotic trigger controlled by hydrogen bonds via a conformational transition. *Chem. Commun.* **14**, 4512–4514 (2009), 10.1039/b904347k.
28. C. Sanders, S. Turkarslan, D. W. Lee, F. Daldal, Cytochrome c biogenesis: The Ccm system. *Trends Microbiol.* **18**, 266–274 (2010).
29. R. G. Kranz, C. Richard-Fogal, J. S. Taylor, E. R. Frawley, Cytochrome c biogenesis: mechanisms for covalent modifications and trafficking of heme and for heme-iron redox control. *Microbiol. Mol. Biol. Rev.* **73**, 510–528 (2009).
30. W. B. Pollock, F. I. Rosell, M. B. Twitchett, M. E. Dumont, A. G. Mauk, Bacterial expression of a mitochondrial cytochrome c. Trimethylation of lys72 in yeast iso-1-cytochrome c and the alkaline conformational transition. *Biochemistry* **37**, 6124–6131 (1998).
31. J. N. Rumbley, L. Hoang, S. W. Englander, Recombinant equine cytochrome c in Escherichia coli: High-level expression, characterization, and folding and assembly mutants. *Biochemistry* **41**, 13894–13901 (2002).
32. R. Feissner, Y. Xiang, R. G. Kranz, Chemiluminescent-based methods to detect subpicomole levels of c-type cytochromes. *Anal. Biochem.* **315**, 90–94 (2003).
33. D. L. Mendez *et al.*, Engineered holocytochrome c synthases that biosynthesize new cytochromes c. *Proc. Natl. Acad. Sci. U.S.A.* **114**, 2235–2240 (2017).
34. Y. Ran *et al.*, Spectroscopic identification of heme axial ligands in HtsA that are involved in heme acquisition by Streptococcus pyogenes. *Biochemistry* **49**, 2834–2842 (2010).
35. J. Jiang *et al.*, Designing inhibitors of cytochrome c/cardiolipin peroxidase complexes: mitochondria-targeted imidazole-substituted fatty acids. *Free Radic. Biol. Med.* **71**, 221–230 (2014).
36. D. L. Brautigan *et al.*, Multiple low spin forms of the cytochrome c ferrihemochrome. EPR spectra of various eukaryotic and prokaryotic cytochromes c. *J. Biol. Chem.* **252**, 574–582 (1977).
37. S. Hirota *et al.*, Cytochrome c polymerization by successive domain swapping at the C-terminal helix. *Proc. Natl. Acad. Sci. U.S.A.* **107**, 12854–12859 (2010).
38. L. J. McClelland *et al.*, Cytochrome c can form a well-defined binding pocket for hydrocarbons. *J. Am. Chem. Soc.* **138**, 16770–16778 (2016).
39. J. Birnbaum *et al.*, A Kelch13-defined endocytosis pathway mediates artemisinin resistance in malaria parasites. *Science* **367**, 51–59 (2020).
40. F. Ariey *et al.*, A molecular marker of artemisinin-resistant *Plasmodium falciparum* malaria. *Nature* **505**, 50–55 (2014).
41. N. F. Gnadig *et al.*, Insights into the intracellular localization, protein associations and artemisinin resistance properties of *Plasmodium falciparum* K13. *PLoS Pathog.* **16**, e1008482 (2020).
42. A. R. Gomes *et al.*, A genome-scale vector resource enables high-throughput reverse genetic screening in a malaria parasite. *Cell Host Microbe* **17**, 404–413 (2015).
43. M. Zhang *et al.*, Uncovering the essential genes of the human malaria parasite *Plasmodium falciparum* by saturation mutagenesis. *Science* **360**, eaap7847 (2018).
44. S. M. Ganesan, A. Falla, S. J. Goldfless, A. S. Nasamu, J. C. Niles, Synthetic RNA-protein modules integrated with native translation mechanisms to control gene expression in malaria parasites. *Nat. Commun.* **7**, 10727 (2016).
45. T. S. Skinner-Adams *et al.*, Cyclization-blocked proguanil as a strategy to improve the antimalarial activity of atovaquone. *Commun. Biol.* **2**, 166 (2019).
46. D. G. Paton *et al.*, Exposing Anopheles mosquitoes to antimalarials blocks *Plasmodium* parasite transmission. *Nature* **567**, 239–243 (2019).
47. G. L. Nixon *et al.*, Targeting the mitochondrial electron transport chain of *Plasmodium falciparum*: new strategies towards the development of improved antimalarials for the elimination era. *Future Med. Chem.* **5**, 1573–1591 (2013).
48. M. A. Phillips *et al.*, A long-duration dihydroorotate dehydrogenase inhibitor (DSM265) for prevention and treatment of malaria. *Sci. Transl. Med.* **7**, 296ra111 (2015).
49. C. D. Goodman, H. D. Buchanan, G. I. McFadden, Is the mitochondrion a good malaria drug target? *Trends Parasitol.* **33**, 185–193 (2017).

50. A. B. Vaidya, M. W. Mather, Mitochondrial evolution and functions in malaria parasites. *Annu. Rev. Microbiol.* **63**, 249–267 (2009).
51. G. G. van Dooren, L. M. Stimmler, G. I. McFadden, Metabolic maps and functions of the *Plasmodium* mitochondrion. *FEMS Microbiol. Rev.* **30**, 596–630 (2006).
52. A. Seidi *et al.*, Elucidating the mitochondrial proteome of *Toxoplasma gondii* reveals the presence of a divergent cytochrome c oxidase. *Elife* **7**, e38131 (2018).
53. J. Krungkrai, The multiple roles of the mitochondrion of the malarial parasite. *Parasitology* **129**, 511–524 (2004).
54. H. Ke *et al.*, Genetic investigation of tricarboxylic acid metabolism during the *Plasmodium falciparum* life cycle. *Cell Rep.* **11**, 164–174 (2015).
55. A. E. Maclean, J. A. Hayward, D. Huet, G. G. van Dooren, L. Sheiner, The mystery of massive mitochondrial complexes: The apicomplexan respiratory chain. *Trends Parasitol.* **38**, 1041–1052 (2022).
56. J. A. Hayward, G. G. van Dooren, Same same, but different: Uncovering unique features of the mitochondrial respiratory chain of apicomplexans. *Mol. Biochem. Parasitol.* **232**, 111204 (2019).
57. A. E. Maclean *et al.*, Complexome profile of *Toxoplasma gondii* mitochondria identifies divergent subunits of respiratory chain complexes including new subunits of cytochrome bc1 complex. *PLoS Pathog.* **17**, e1009301 (2021).
58. J. A. Hayward, E. Rajendran, S. M. Zwahlen, P. Faou, G. G. van Dooren, Divergent features of the coenzyme Q: Cytochrome c oxidoreductase complex in *Toxoplasma gondii* parasites. *PLoS Pathog.* **17**, e1009211 (2021).
59. E. Glaser, P. Dessi, Integration of the mitochondrial-processing peptidase into the cytochrome bc1 complex in plants. *J. Bioenerg. Biomembr.* **31**, 259–274 (1999).
60. O. Gakh, P. Cavadini, G. Isaya, Mitochondrial processing peptidases. *Biochim. Biophys. Acta* **1592**, 63–77 (2002).
61. M. D. Crivellone, M. A. Wu, A. Tzagoloff, Assembly of the mitochondrial membrane system. Analysis of structural mutants of the yeast coenzyme QH2-cytochrome c reductase complex. *J. Biol. Chem.* **263**, 14323–14333 (1988).
62. M. Heidorn-Czarna, A. Maziak, H. Janska, Protein processing in plant mitochondria compared to yeast and mammals. *Front. Plant Sci.* **13**, 824080 (2022).
63. M. J. Gardner *et al.*, Genome sequence of the human malaria parasite *Plasmodium falciparum*. *Nature* **419**, 498–511 (2002).
64. G. J. Morgan, Emile Zuckerkandl, Linus Pauling, and the molecular evolutionary clock, 1959–1965. *J. Hist. Biol.* **31**, 155–178 (1998).
65. W. M. Fitch, The molecular evolution of cytochrome c in eukaryotes. *J. Mol. Evol.* **8**, 13–40 (1976).
66. J. R. Mattoon, F. Sherman, Reconstitution of phosphorylating electron transport in mitochondria from a cytochrome c-deficient yeast mutant. *J. Biol. Chem.* **241**, 4330–4338 (1966).
67. T. M. Laz, D. F. Pietras, F. Sherman, Differential regulation of the duplicated isocytochrome c genes in yeast. *Proc. Natl. Acad. Sci. U.S.A.* **81**, 4475–4479 (1984).
68. S. M. Sidik *et al.*, A Genome-wide CRISPR screen in *Toxoplasma* identifies essential apicomplexan genes. *Cell* **166**, 1423–1435.e1412 (2016).
69. M. Kellis, B. W. Birren, E. S. Lander, Proof and evolutionary analysis of ancient genome duplication in the yeast *Saccharomyces cerevisiae*. *Nature* **428**, 617–624 (2004).
70. C. I. Wu *et al.*, Evolution of cytochrome c genes and pseudogenes. *J. Mol. Evol.* **23**, 61–75 (1986).
71. S. Kumar *et al.*, TimeTree 5: An expanded resource for species divergence times. *Mol. Biol. Evol.* **39**, msac174 (2022).
72. E. Bushell *et al.*, Functional profiling of a *Plasmodium* genome reveals an abundance of essential genes. *Cell* **170**, 260–272.e268 (2017).
73. M. E. Hillenmeyer *et al.*, The chemical genomic portrait of yeast: Uncovering a phenotype for all genes. *Science* **320**, 362–365 (2008).
74. Z. Zhang, M. Gerstein, The human genome has 49 cytochrome c pseudogenes, including a relic of a primordial gene that still functions in mouse. *Gene* **312**, 61–72 (2003).
75. Y. Hong, J. Muenzner, S. K. Grimm, E. V. Pletneva, Origin of the conformational heterogeneity of cardiolipin-bound cytochrome C. *J. Am. Chem. Soc.* **134**, 18713–18723 (2012).
76. V. E. Kagan *et al.*, Cytochrome c acts as a cardiolipin oxygenase required for release of proapoptotic factors. *Nat. Chem. Biol.* **1**, 223–232 (2005).
77. M. J. Lopez-Barragan *et al.*, Directional gene expression and antisense transcripts in sexual and asexual stages of Plasmodium falciparum. *BMC Genomics* **12**, 587 (2011).
78. E. Real *et al.*, A single-cell atlas of *Plasmodium falciparum* transmission through the mosquito. *Nat. Commun.* **12**, 3196 (2021).
79. J. M. Matz, C. Goosmann, K. Matuschewski, T. W. A. Kooij, An unusual prohibitin regulates malaria parasite mitochondrial membrane potential. *Cell Rep.* **23**, 756–767 (2018).
80. H. Ke *et al.*, The heme biosynthesis pathway is essential for *Plasmodium falciparum* development in mosquito stage but not in blood stages. *J. Biol. Chem.* **289**, 34827–34837 (2014).
81. C. D. Goodman *et al.*, Parasites resistant to the antimalarial atovaquone fail to transmit by mosquitoes. *Science* **352**, 349–353 (2016).
82. H. S. Wong, P. A. Dighe, V. Mezera, P. A. Monternier, M. D. Brand, Production of superoxide and hydrogen peroxide from specific mitochondrial sites under different bioenergetic conditions. *J. Biol. Chem.* **292**, 16804–16809 (2017).
83. F. L. Muller, Y. Liu, H. Van Remmen, Complex III releases superoxide to both sides of the inner mitochondrial membrane. *J. Biol. Chem.* **279**, 49064–49073 (2004).
84. P. A. Sigala, J. R. Crowley, J. P. Henderson, D. E. Goldberg, Deconvoluting heme biosynthesis to target blood-stage malaria parasites. *Elife* **4**, e09143 (2015).
85. T. E. Wellems *et al.*, Chloroquine resistance not linked to mdr-like genes in a *Plasmodium falciparum* cross. *Nature* **345**, 253–255 (1990).
86. T. Ponnudurai, A. D. Leeuwenberg, J. H. Meuwissen, Chloroquine sensitivity of isolates of *Plasmodium falciparum* adapted to in vitro culture. *Trop. Geogr. Med.* **33**, 50–54 (1981).
87. M. Okada, P. Guo, S. A. Nalder, P. A. Sigala, Doxycycline has distinct apicoplast-specific mechanisms of antimalarial activity. *Elife* **9**, e60246 (2020).
88. M. Okada *et al.*, Critical role for isoprenoids in apicoplast biogenesis by malaria parasites. *Elife* **11**, e73208 (2022).
89. P. Emsley, B. Lohkamp, W. G. Scott, K. Cowtan, Features and development of Coot. *Acta Crystallogr. D Biol. Crystallogr.* **66**, 486–501 (2010).
90. P. D. Adams *et al.*, PHENIX: A comprehensive Python-based system for macromolecular structure solution. *Acta Crystallogr. D Biol. Crystallogr.* **66**, 213–221 (2010).
91. J. A. Wohlschlegel, Identification of SUMO-conjugated proteins and their SUMO attachment sites using proteomic mass spectrometry. *Methods Mol. Biol.* **497**, 33–49 (2009).
92. D. E. Goldberg, P. A. Sigala, Plasmodium heme biosynthesis: To be or not to be essential? *PLoS Pathog.* **13**, e1006511 (2017).